THE JOURNAL OF PHYSICAL CHEMISTRY C

Article

Cite This: J. Phys. Chem. C 2018, 122, 307−314

pubs.acs.org/JPCC

Adsorption of CO_2 and Facile Carbonate Formation on $BaZrO_3$ Surfaces

Jonathan M. Polfus,*[†,§] Bilge Yildiz,[‡,§] Harry L. Tuller,[§] and Rune Bredesen[†]

[†]SINTEF Industry, Sustainable Energy Technology, P.O. Box 124 Blindern, NO-0314 Oslo, Norway

[‡]Department of Nuclear Science and Engineering and [§]Department of Material Science and Engineering, Massachusetts Institute of Technology, 77 Massachusetts Avenue, Cambridge, Massachusetts 02139, United States

ABSTRACT: The adsorption of CO_2 and CO on $BaZrO_3$ (0 0 1) was investigated by first-principles calculations with a focus on the BaO termination. CO_2 was found to strongly chemisorb on the surface by formation of carbonate species with an adsorption enthalpy of up to −2.25 eV at low coverage and −1.05 eV for a full monolayer. An adsorption entropy of -8.8×10^{-4} eV K^{-1} was obtained from the vibrational properties of the adsorbates. Surface coverages were evaluated as a function of temperature and CO_2 partial pressure, and the obtained coverage under 1 bar CO_2 was more than 0.8 at 1000 K (conditions relevant for steam methane reforming). The fully saturated surface was stable up to about 400 K under ambient atmosphere, i.e., 400 ppm of CO_2. The initial stage of $BaCO_3$ formation was evaluated according to migration of barium to the carbonate overlayer, which was found to result in a significant stabilization of the system. The barium migration was found to be essentially unobstructed with a barrier of only ∼5 meV. In light of the stability of carbonate adsorbates at the surface, the prospect of bulk dissolution of carbonate species was evaluated but ultimately found to be negligible in acceptor-doped $BaZrO_3$.

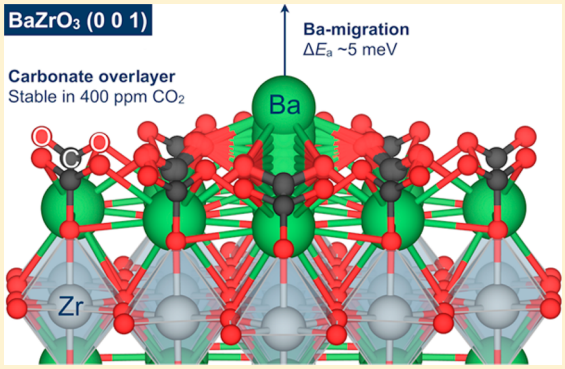

1. INTRODUCTION

Perovskite oxides are utilized as functional materials in the presence of carbon-containing atmospheres for several applications such as solid oxide fuel cells with internal reforming of hydrocarbons, membrane reactors, thermochemical reduction of CO_2 to liquid fuels, catalytic oxidation of CO, and gas sensing.[1−6] The surface chemistry and potential reactivity of CO_2 and CO with oxide surfaces is therefore of interest in order to understand how the equilibrium surface is affected in terms of, for instance, ionic conductivity, oxygen exchange, or catalytic activity.

Proton-conducting oxides, such as acceptor-doped $BaZrO_3$, tend to contain basic cations since the basicity of the oxide correlates with an increased exothermicity of proton incorporation according to the hydration reaction.[7,8] These oxides are therefore prone toward reaction with CO_2 leading to carbonate formation. Reaction with CO_2 is favored at lower temperatures due to the negative entropy change for the reaction of gaseous CO_2 to solid carbonate. Reactivity toward CO_2 therefore becomes increasingly important in the search for lowering the operating temperature of proton ceramic fuel cells (PCFC) toward intermediate temperatures of less than 500 °C.[9] Furthermore, Malerød-Fjeld et al. recently demonstrated an electrochemical membrane reactor for production of hydrogen from steam methane reforming, exposing the $BaZrO_3$-based electrolyte and electrodes to CO_2-rich atmospheres at 800 °C and 10 bar.[10]

The chemical stability of bulk $BaZrO_3$ in CO_2-containing atmospheres with respect to $BaCO_3$ has been demonstrated experimentally as expected based on thermodynamic evaluation.[11,12] However, recent studies have shown that the surface exhibits some reactivity and $BaCO_3$ formation, not by decomposition of the perovskite but by accommodating barium deficiency in the surface and subsurface of the material.[13] Carbonates are commonly observed on the surface of similar oxides exposed to ambient atmosphere which contains about 4×10^{-4} bar CO_2 (400 ppm).

Carbon dioxide can adsorb as a linear physisorbed molecule or by chemisorption of bent CO_2 molecules or carbonate species, CO_3^{2-}. Mei et al. investigated the adsorption of CO_2 on the BaO (0 0 1) surface, which is structurally equivalent to the BaO-terminated $BaZrO_3$ (0 0 1) surface.[14] CO_2 was found to adsorb most favorably as monodentate carbonate species, i.e., bound to one surface oxide ion, with adsorption energies of up to −2.0 eV at low coverage. For MgO and CaO (0 0 1) surfaces, Jensen et al. obtained monodentate CO_2 adsorption energies of −1.6 and −1.0 eV and up to −2.3 eV on step sites.[15] In comparison, adsorption enthalpies of −1.8 and −1.3 eV have been obtained by microcalorimetry for polycrystalline MgO[16] and monocrystalline CaO (0 0 1), respectively.[17]

Received: August 17, 2017
Revised: December 15, 2017
Published: January 3, 2018

DOI: 10.1021/acs.jpcc.7b08223
J. Phys. Chem. C 2018, 122, 307−314

Similar monodentate CO_2 adsorption geometries have been reported for both A- and B-site terminated (0 0 1) perovskite surfaces with somewhat lower adsorption energies in the range of −1.0 to −1.6 eV for $SrTiO_3$,[18] $LaMnO_3$,[19] and $K_{1-y}Na_yTa_{1-x}Nb_xO_3$.[20] The measured adsorption enthalpy for $SrTiO_3$ (0 0 1) was −1.1 eV in good agreement with theoretical value for the pristine surface, −1.0 eV.[21] For the computational studies on $LaMnO_3$ and $SrTiO_3$, the strongest CO_2 adsorption energies were obtained at neutral F-centers at the surface, i.e., V_O^X in Kröger−Vink notation,[22] where the adsorbate appeared as a CO_2^- or CO_2^{2-} species with carbon residing close to the vacant oxide ion position.[19,23] While the adsorption energies were about −2 eV, this adsorption mechanism necessitates the presence of $V_O^\times$ and can therefore be considered most relevant in selected heavily reduced systems. The adsorption and activation of CO_2 has been studied for several surface terminations of pristine and reduced ceria. In all cases, the most stable adsorbates were carbonate species in monodentate or tridentate configurations with adsorption energies ranging from −0.31 to −1.93 eV.[24−26]

Adsorption of carbon monoxide on oxide surfaces has received comparatively less attention. CO adsorption typically involves rather weak physisorption with carbon directed toward the surface cation,[27] while bidentate carbonate adsorbates can form on surfaces where C can bridge two surface oxide ions.[4]

The present work deals with adsorption of CO_2 and CO on the (0 0 1) surface of $BaZrO_3$ with focus on the BaO termination, which is the most stable termination.[28,29] The ZrO_2 termination was also considered which could be relevant for Ba-deficient material and for comparison with other oxides. Density functional theory (DFT) calculations were utilized to assess the adsorption energetics and the vibrational properties and electronic structure of the adsorbates. Furthermore, surface coverages of the adsorbates were evaluated as a function of environmental variables. Considering the favorable adsorption energetics and geometry of surface carbonate species, $BaCO_3$ formation was evaluated. The prospect of interstitial carbon in the bulk $BaZrO_3$ structure was also investigated on the basis of the thermodynamics of defect formation.

2. COMPUTATIONAL DETAILS

DFT calculations were performed using the projector-augmented wave method as implemented in VASP with the PBE-generalized gradient approximation functional.[30−32] The plane-wave cutoff was 500 eV, and the k-point sampling was equivalent to 8 × 8 × 8 for the cubic $BaZrO_3$ unit cell. The atomic positions and cell parameters were converged to less than 0.02 eV $Å^{-1}$ (0.02−0.04 eV $Å^{-1}$ including adsorbates due to some sensitive configurations). Selected calculations were performed with the semiempirical van der Waals correction due to Grimme (DFT+D2).[33]

Surfaces of $BaZrO_3$ (0 0 1) were constructed as symmetric 11-layer BaO- and ZrO_2-terminated slabs separated by a 25 Å vacuum layer. Adsorbates were considered in cells of 2 × 2 to 4 × 4 expansion in the *ab*-plane (up to 432 atoms) in order to evaluate different levels of surface coverage. The adsorbates were arranged in several symmetrically inequivalent configurations in order to obtain the minimum energy configuration and introduced on both sides of the slabs to avoid dipole formation. The adsorption thermodynamics were evaluated based on the adsorption energy, configurational entropy and vibrational properties of the adsorbates. The vibrational frequencies were obtained according to the finite displacement method implemented in VASP with four 0.015 Å displacements of the vibrating species along all Cartesian directions. The adsorption energy, ΔE_i^{ads}, was calculated as the total energy differences of the adsorption reactions. The vibrational entropy of the adsorbates, S_i^{vib}, were obtained from the normal frequencies of the adsorbates according to

$$S_i^{vib} = k \sum_j \left(\frac{\beta_j}{\exp(\beta_j) - 1} - \ln(1 - \exp(-\beta_j)) \right) \quad (1)$$

where $\beta_j = h\nu_j/kT$ is the vibrational energy for the adsorbate with vibrational frequency ν_j.[34] The configurational entropy of the adsorbate for a given surface coverage, Θ_i, was calculated according to

$$S_i^{conf} = k(\Theta_i \ln(\Theta_i) + (1 - \Theta_i) \ln(\Theta_i)) \quad (2)$$

The adsorption entropies, ΔS_i^{ads}, were obtained with the gaseous reference states taken from thermochemical tables.[35] For comparison, the standard entropy of CO_2 obtained with the calculated vibrational frequencies and the translational/rotational contributions from statistical thermodynamics was within 0.14% of the tabulated value, 2.22×10^{-3} eV K^{-1}. The equilibrium constant of the adsorption reactions was given by

$$K = \exp\left(-\frac{\Delta H_i^{ads}}{kT}\right) \exp\left(\frac{\Delta S_i^{ads}}{T}\right) \quad (3)$$

where ΔH_i^{ads} includes the surface coverage dependent adsorption energy, $\Delta E_i^{ads}(\Theta_i)$ and the zero-point energy (ZPE) contribution. For the adsorption reaction $CO_2(g) + * = CO_{2,ad}$, where * denotes an empty adsorption site, the surface coverage without competitive adsorption is given by

$$\Theta_{CO_2} = \frac{\sqrt{Kp_{CO_2}}}{1 + \sqrt{Kp_{CO_2}}} \quad (4)$$

The surface coverage was calculated numerically from eq 1 to 4 by variation over an initial surface coverage (from 0 to 1) until the initial and calculated coverage converged within an accuracy of 10^{-3}.

Segregation of barium from the perovskite surface was evaluated in the presence of carbonate adsorbates at initial stages of $BaCO_3$ formation on the surface. These calculations were performed in 3 × 3 expanded 11-layer slabs, and the potential energy profile for the migration of barium was calculated using the nudged elastic band method.

The possibility of carbon dissolution into the bulk perovskite structure was evaluated according to the Gibbs formation energy, ΔG_{def}^f, of carbon interstitials

$$\Delta G_{def}^f = E_{def}^{tot} - E_{bulk}^{tot} + \sum_i n_i\mu_i + q\mu_e \quad (5)$$

where E_{def}^{tot} and E_{bulk}^{tot} are the total energies of the defective and bulk cell, n_i is the number and type of atomic species exchanged with the system upon defect formation, μ_e is the Fermi level, and q is the effective charge of the defect. The environmental conditions are defined by the atomic chemical potentials, μ_i. The chemical potentials of the gases were obtained from

DOI: 10.1021/acs.jpcc.7b08223
J. Phys. Chem. C 2018, 122, 307−314

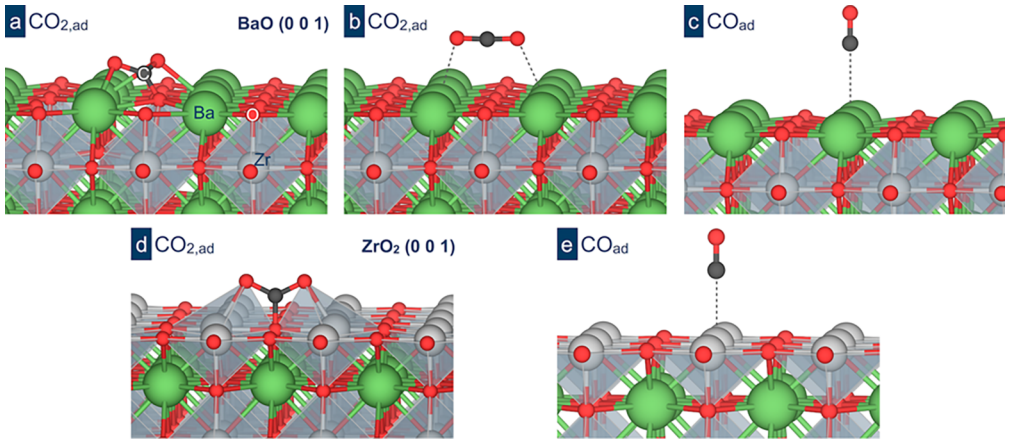

Figure 1. Adsorption geometries of CO_2 and CO on $BaZrO_3$ (0 0 1): BaO termination (a–c) and ZrO_2 termination (d, e). The dihedral angle of the carbonate adsorbate with respect to the BaO plane in (a) was 52°.

$$\mu_i(T, p_i) = \mu_i^\circ + kT \ln\left(\frac{p_i}{p^\circ}\right) \tag{6}$$

where μ_i° was taken as the total energies of the respective molecules and the equilibrium partial pressures, p_i, were calculated from thermochemical equilibria.[36] The chemical potentials of the $BaZrO_3$ constituent cations were defined according to Ba-rich conditions with $BaCO_3$ and CO_2 as the thermodynamic limits, i.e.

$$\mu_{Ba} = \mu_{BaCO_3} - \mu_C - 3\mu_O \tag{7}$$

$$\mu_{Zr} = \mu_{BaZrO_3} - \mu_{Ba} - 3\mu_O \tag{8}$$

$$\mu_C = \mu_{CO_2} - 2\mu_O \tag{9}$$

The binding energies between carbon interstitials and cation vacancies were calculated as the enthalpy of the defect association reaction, e.g.,

$$C_i^{4\bullet} + V_{Zr}^{4\prime} = (C_iV_{Zr})^{\times} \tag{10}$$

$$C_i^{4\bullet} + (C_iV_{Zr})^{\times} = (2C_iV_{Zr})^{4\bullet} \tag{11}$$

The stability of the associated defects is representative of carbon substituting for Ba or Zr where C is displaced from the central Ba^{2+} or Zr^{4+} position due to its comparatively small size.

3. RESULTS AND DISCUSSION

3.1. Adsorption Energies. The relaxed adsorbates on BaO- and ZrO_2-terminated $BaZrO_3$ (0 0 1) surfaces are shown in Figure 1 with corresponding adsorption energies in listed in Table 1. Most notably, the CO_2 molecule may chemisorb on both terminations by forming a surface carbonate species, denoted $CO_{2,ad}$ (Figure 1a,d). The carbonate adsorbates are by far the most stable with adsorption energies of −2.20 and −1.93 eV for the BaO and ZrO_2 termination, respectively. These carbonate adsorption energies are more exothermic than values reported for other perovskites and CeO_2, −0.31 eV to −2.0 eV, as described in the Introduction. Although carbonate adsorbates on perovskite surfaces are often denoted *monodentate* due to the single surface oxide ion bond, the additional bonds between oxygen and the surface cations imply *tridentate* to be an appropriate description on $BaZrO_3$ (0 0 1) (Figure 1a,d).[37]

Table 1. Calculated Adsorption Energy of CO_2 and CO on BaO- and ZrO_2-Terminated $BaZrO_3$ (0 0 1)

			ΔE^{ads} (eV)	
molecule	adsorption	coordination	BaO	ZrO_2
CO_2	chemisorbed	carbonate	−2.20	−1.93
	physisorbed	O–Ba bond	−0.27	
CO	physisorbed	C–Ba/Zr bond	−0.10	−0.34

The adsorption energy of physisorbed CO_2 on the BaO-terminated surface (Figure 1b) was −0.27 eV, which is similar to that reported for CeO_2 (1 1 0), −0.26 eV.[24] The O–Ba bond lengths were 5.24 Å. Carbon monoxide adsorbates were found to be most stable with carbon directed toward the surface cations (Figure 1c,e), which exhibited rather low adsorption energies of −0.10 and −0.34 eV for the BaO and ZrO_2 termination, respectively. The bond lengths to the surface were 2.60 Å for C–Zr and 3.27 Å for C–Ba (2.60 and 3.31 Å with DFT + D2). It was determined that CO cannot chemisorb to a surface oxide ion, which means that CO_2 does not adsorb directly into a surface oxygen vacancy.

3.2. Electronic Structure and Geometry. The electronic structure of adsorbed carbonate species on the BaO-terminated surface is compared to that of bulk $BaCO_3$ in Figure 2. The occupied C 2s and 2p states are quite similar between the adsorbate and bulk carbonate phase, with a slightly less distinct C 2p triplet peak for the latter. Furthermore, carbon exhibits a significant overlap with O 2p states according to the sp^2 hybridization of the carbonate ion. The local structural environments around the carbonate species are also very similar in terms of coordination and bond lengths (Figure 2 inset), with the main differences in C–O–Ba bond angles originating from the different symmetry of $BaCO_3$ and the $BaZrO_3$ surface. The C–O bond length was 1.30 Å in $BaCO_3$ and 1.28 Å for the adsorbate (1.35 Å to the surface oxide ion). The Ba–O bond lengths were 2.76 and 2.91 Å in $BaCO_3$ and 2.73 Å for the carbonate adsorbate (3.02 Å to the Ba coordinated to both CO_2 oxide ions). The bond angles of the carbonate adsorbate were 122.9° and 118.4° involving the surface oxide ion, compared to 120° in $BaCO_3$.

3.3. Vibrational Entropy. The main vibrational frequencies of the carbonate group are listed in Table 2 for bulk $BaCO_3$, chemisorbed CO_2 as well as an interstitial carbon

DOI: 10.1021/acs.jpcc.7b08223
J. Phys. Chem. C 2018, 122, 307–314

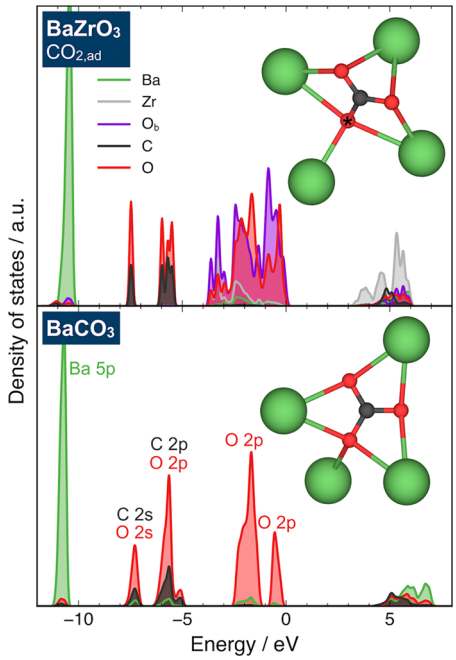

Figure 2. Site projected electronic density of states of BaO-terminated $BaZrO_3$ (0 0 1) with CO_2 adsorbed as a carbonate species (top) and $BaCO_3$ (bottom). The insets show the local cation coordination around the carbonate species. For $BaZrO_3$, O_b refers to the lattice oxide ions, and the surface oxide ion is marked with an asterisk. The $BaZrO_3$ valence band maximum was referenced to 0 eV, and the C 1s core level was aligned between the two materials. The peaks are labeled according to the main contributing orbitals which were the same in both materials.

Table 2. Calculated Vibrational Frequencies Associated with the Carbonate Group for Bulk $BaCO_3$ P*mcn*, Chemisorbed CO_2 on BaO-Terminated $BaZrO_3$ (0 0 1), and an Interstitial Carbon Defect Described in Section 3.4

frequency (cm^{-1})			
$BaCO_3$	$CO_{2,ad}$	$(C_i V_{Zr})^X$	mode
1412	1498	1332	ν_3, asymmetric stretch
1385	1303		
1044	1009	1027	ν_1, symmetric stretch
841	830	807	ν_2, out-of-plane bend
689	700	625	ν_4, in-plane bend
649	646		

defect complex described in section 3.4. The calculated vibrational frequencies for $BaCO_3$ were 0.5−2% lower than experimental values.[38] The frequencies of the carbonate modes are quite similar for all cases, which indicates a similar chemical nature of the carbonate specie in the quite different environments.

The vibrational entropy of adsorption and the ZPE contribution to the enthalpy of adsorption was obtained from the vibrational frequencies of chemisorbed CO_2 (Table 2), molecular CO_2, and the $BaZrO_3$ surface oxide ion based on eq 1. ΔZPE of chemisorption was calculated to be 0.117 eV per CO_2. The calculated vibrational entropy of chemisorption, -8.8×10^{-4} eV K^{-1} per CO_2, was found to be within the range of values obtained for various carbonate adsorbates on MgO (0 0 1).[37]

3.4. Surface Coverage. The adsorption energy of carbonate species was evaluated up to full coverage for different adsorption geometries and configurations on the BaO-terminated surface. In comparison with the isolated carbonate adsorbate in Figure 1a which exhibited an adsorption energy of −2.20 eV (Θ_{CO2} = 0.06), the adsorption energy was −0.84 eV (per CO_2) for full coverage of the same adsorption geometry (Figure 3a). The most stable configuration at full coverage was obtained for a cell with 3 × 3 periodicity (Figure 3b), which exhibited an adsorption energy of −1.05 eV with slightly different adsorbate geometries as highlighted by the arrows in Figure 3b. The adsorption energy was −1.64 eV at half coverage (Figure 3a) and −1.93 eV at quarter coverage, and the adsorption energies thereby exhibit a strong linear relationship with coverage (R^2 = 0.999) according to $\Delta H^{ads}_{CO2} = (-2.25 + 1.21\Theta_{CO2}) + \Delta ZPE$, $0 < \Theta_{CO2} \leq 1$.

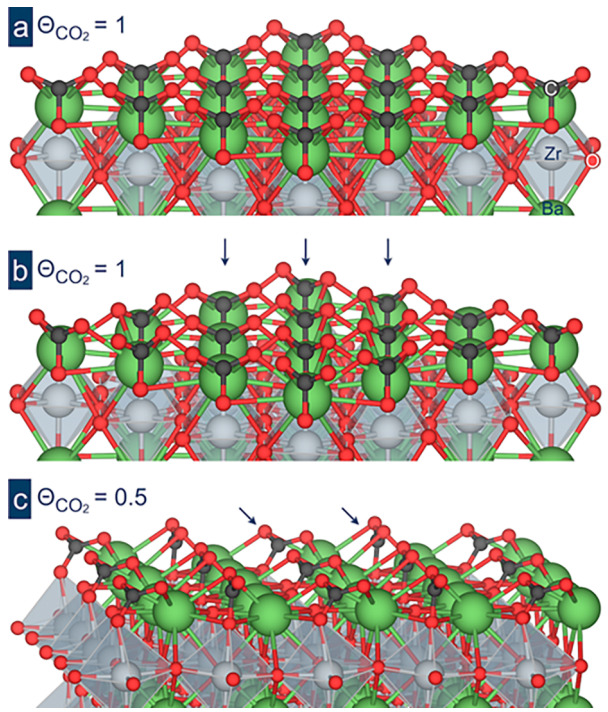

Figure 3. Carbonate adsorbates on BaO-terminated $BaZrO_3$ (0 0 1) at full coverage (a) and (b) and half coverage (c). The arrows in (b) and (c) indicate rows of different adsorption geometries and orientations.

Figure 4 shows the calculated surface coverage of carbonate adsorbate on the BaO-terminated surface as a function of temperature at selected CO_2 partial pressures from 1 bar to 400 ppm. The calculated coverage remains quite significant throughout the temperature range even for 400 ppm of CO_2. The figure also shows the corresponding adsorption enthalpy as the CO_2 coverage varies with temperature. Competitive adsorption of physisorbed CO_2 or CO was considered negligible due to the significantly lower adsorption energies (Table 1).

Interactions between the carbonate adsorbates and other surface species was investigated for the most significant surface point defects on $BaZrO_3$ (0 0 1), protons, and oxygen vacancies.[39] A quite substantial CO_2 coverage of 0.5 was employed together with surface defect concentrations of 0.25 of the surface oxide ions. The adsorption energy of CO_2 for this coverage (−1.64 eV) was essentially unchanged with a proton associated with a neighboring surface oxide ion site

DOI: 10.1021/acs.jpcc.7b08223
J. Phys. Chem. C 2018, 122, 307−314

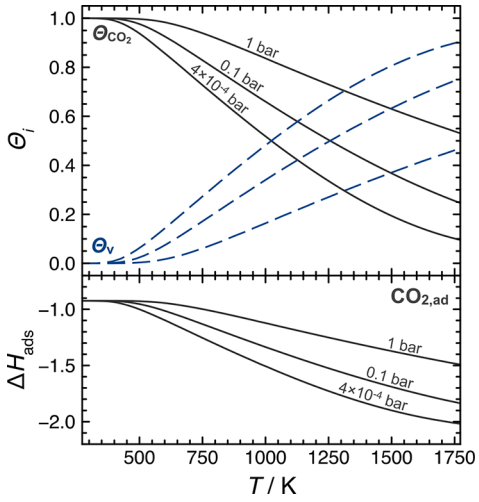

Figure 4. Surface coverage of CO_2 and vacant sites on the BaO-terminated $BaZrO_3$ (0 0 1) surface as a function of temperature for different p_{CO2} (top) and the corresponding CO_2 adsorption enthalpy (per CO_2) as the coverage varies as a function of temperature (bottom).

(−1.65 eV). However, the carbonate and hydroxide species were stabilized by 0.31 eV when residing on adjacent sites as shown in Figure 5a resulting in an average adsorption energy of

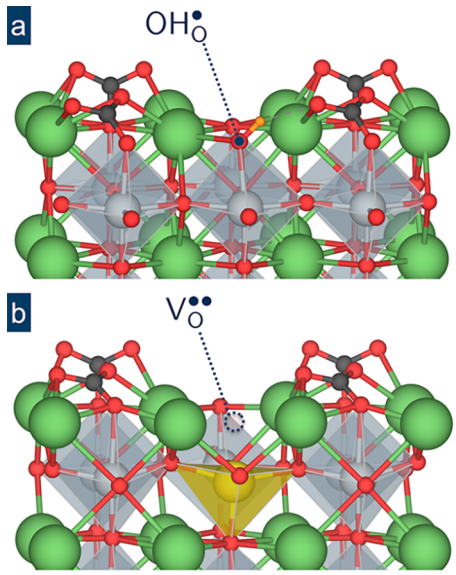

Figure 5. CO_2 adsorbates (Θ_{CO2} = 0.5) in the presence of a next-neighbor surface proton (a) and a surface oxygen vacancy (b) corresponding to a concentration of 0.25 of the surface oxide ions on BaO-terminated $BaZrO_3$ (0 0 1). The surface oxygen vacancy was associated with a Y'_{Zr} acceptor (yellow).

−1.81 eV per CO_2 for that configuration. The proton relaxed toward one of the carbonate oxide ions, but transfer of the proton to this oxide ion resulted in partial desorption of the carbonate species and destabilization of the adsorbates by 1.22 eV. In the presence of a surface oxygen vacancy (Figure 5b) the CO_2 adsorption became more exothermic, −2.02 per CO_2 compared to −1.64 eV for the pristine surface.

Another important aspect of the role of surface oxygen vacancies relates to site occupancy, i.e., chemisorbed CO_2 and oxygen vacancies compete for the same surface oxide ion sites. The relative stability of carbonate adsorbates and surface oxygen vacancies therefore has to be considered. In this respect, the calculated surface segregation energy for oxygen vacancies, −0.42 eV for the BaO-terminated (0 0 1) surface,[40] is significantly less exothermic than the adsorption energies even at full coverage. It is therefore reasonable to assert that the presence of surface oxygen vacancies would have a limited effect on the calculated CO_2 coverages, particularly for Θ_{CO2} < 1, e.g., > 500 K at 1 bar CO_2.

3.5. Barium Segregation. The initial stage of $BaCO_3$ formation was investigated for the BaO-terminated surface with the full carbonate overlayer, i.e., Θ_{CO2} = 1 (Figure 3b), which is predicted to be stable up to about 600 K in 1 bar CO_2 and 400 K in 400 ppm of CO_2 (Figure 4). $BaCO_3$ formation was considered to be initiated by outward relaxation/migration of barium to the outer surface of the carbonate overlayer, thereby leaving a barium vacancy in the terminating BaO-layer. Formation of the barium adatom−vacancy pair resulted in a large stabilization of the system by −1.3 eV (Figure 6a). Furthermore, the calculated minimum energy path for barium migration reveals an essentially unobstructed migration process (within 5 meV for the first 0.4 Å, Figure 6b).

3.6. Bulk Carbon Dissolution. The possibility of carbon dissolution into the bulk perovskite structure was evaluated and a relatively stable configuration was identified in which interstitial carbon bonds to three lattice oxide ions to form carbonate species with C−O bond lengths of 1.30 Å. The carbon interstitial, $C_i^{4\bullet}$, exhibited strong steric interaction with the neighboring cations, and was therefore found to be significantly stabilized when associated with cation vacancies as shown in Figure 7. The binding energies between the defects were −1.43 eV and −1.63 eV for association between V''_{Ba} and the first and second $C_i^{4\bullet}$, respectively, and −6.09 eV and −5.37 eV for association between $V^{4\prime}_{Zr}$ and the first and second $C_i^{4\bullet}$, respectively (eqs 10 and 11). It should be noted that the very large binding energies in the latter case may be ascribed to the rather low stability of the isolated zirconium vacancy, while the carbon interstitials form bonds to all of the oxide ions previously bound in the Zr-octahedra (Figure 7b).

Figure 7c shows the calculated Gibbs formation energies of the various carbon interstitials in comparison with intrinsic defects and Y-acceptors. The equilibrium Fermi level is highlighted at around 1 eV which corresponds to the predominating electroneutrality condition $[Y'_{Zr}] = 2[V_O^{\bullet\bullet}]$. Under these conditions, the Gibbs formation energy of most stable carbon related defect, $(2C_i\, V_{Zr})^{4\bullet}$, is higher by several eV which would correspond to a minute concentration. Furthermore, $V_O^{\bullet\bullet}$ remains the predominating charge compensating defect for Y'_{Zr} under all conditions due to the relationship between the chemical potentials of carbon and oxygen through eq 9. Thus, the concentrations of the considered carbon defects would be negligible under equilibrium conditions according to these results. Nevertheless, the considered carbon defects could be incorporated into perovskite oxides by physical methods such as carbon ion implantation.

4. DISCUSSION

CO_2 exhibits significantly exothermic adsorption enthalpies of up to −2.25 eV at low coverage by formation of surface carbonate species on BaO-terminated $BaZrO_3$ (0 0 1). The adsorption enthalpy further follows a linear behavior with coverage, resulting in a quite exothermic adsorption enthalpy

DOI: 10.1021/acs.jpcc.7b08223
J. Phys. Chem. C 2018, 122, 307−314

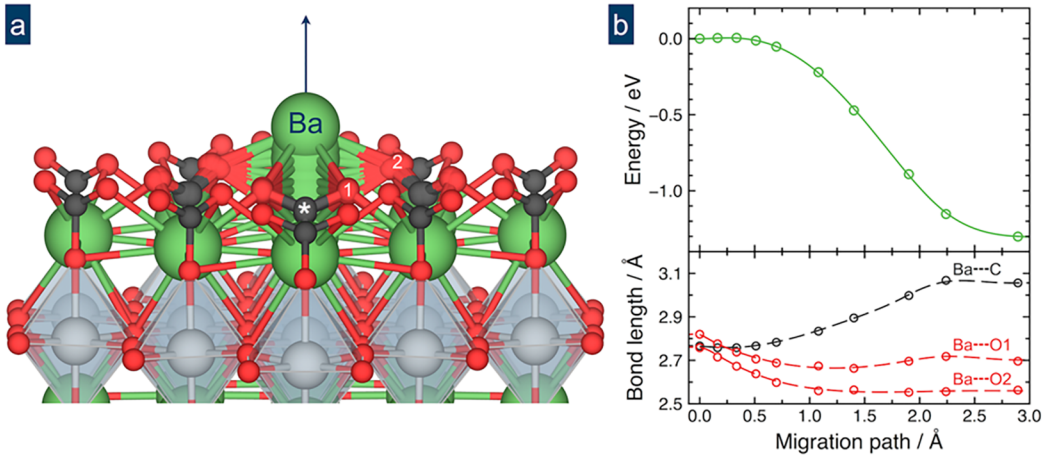

Figure 6. Superimposed images of Ba migration from the BaO-terminated $BaZrO_3$ (0 0 1) surface to the outer surface of the carbonate overlayer (a) and the corresponding energy profile and bond lengths along the migration path from the NEB calculation (b).

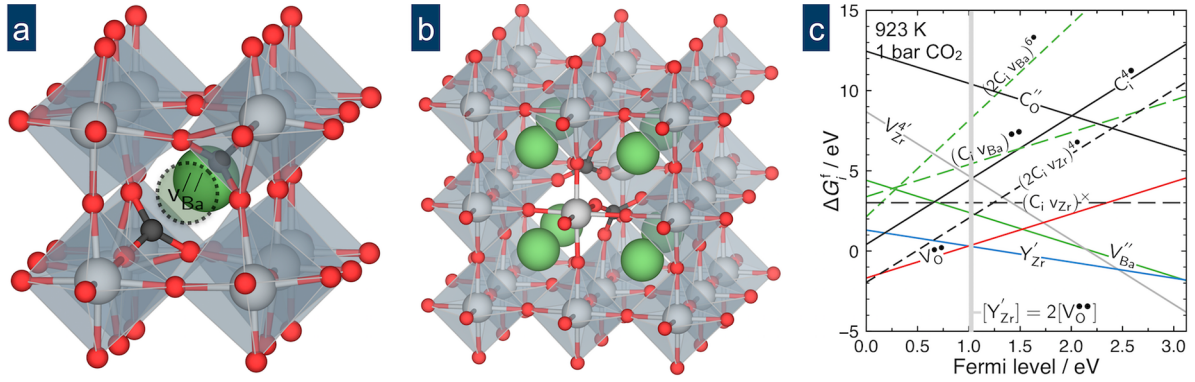

Figure 7. Relaxed structure of two-carbon interstitials in $BaZrO_3$ bound to lattice oxide ions as carbonate species associated with a barium vacancy (a) and zirconium vacancy (b) and Gibbs formation energies of carbon related defects and other relevant defects (c). The carbon interstitial was found to be stable only in the 4+ charge state as additional electrons added to the system ended up in the conduction band.

of −1.05 eV for full coverage of a carbonate overlayer. Based on the electronic structure and the local structural environment of the carbonate adsorbate on the BaO-terminated surface (Figure 2), it was determined that the carbonate overlayer was chemically similar to bulk $BaCO_3$. In this respect, it is interesting to note that the adsorption enthalpy (at low coverage) approaches the enthalpy of formation of $BaCO_3$ from BaO and CO_2, −2.77 eV.

Due to the strong CO_2 adsorption energy, the calculated absorption equilibrium resulted in a significant coverage of more than 0.8 at 1000 K (Figure 4), which are relevant operating conditions for steam reforming membrane reactors. Furthermore, according to the present results, the equilibrium state of BaO-terminated $BaZrO_3$ surfaces under ambient atmospheres (400 ppm of CO_2), up to about 400 K, is the fully saturated surface with a carbonate overlayer that may be considered analogous to $BaCO_3$. The considerable exothermic adsorption energy for the BaO-terminated surface serves as an additional thermodynamic driving force for stabilizing the A-site BaO termination. These results may further apply to similar perovskites and probably be most applicable to perovskites with basic A-site cations that form stable bulk carbonate phases, such as strontium.

In terms of the functional properties of $BaZrO_3$-based electrolytes in CO_2-containing atmospheres, the presence of a carbonate overlayer can be expected to be detrimental to surface reactions such as proton incorporation due to the significantly lower stability of protons associated with the carbonate oxide ions compared to the surface. The presence of carbonate species may therefore, in part, be responsible for an apparently slow surface reaction, rather than intrinsic electrode kinetics or space-charge effects.[39] However, the typical primary surface reaction sites on an electrode or triple phase boundary may be less prone to CO_2 adsorption and thereby be less affected. Furthermore, the competitive adsorption of CO_2 and H_2O under relevant methane reforming conditions may significantly affect the CO_2 coverages.

The onset of $BaCO_3$ formation, as investigated by migration of barium from the terminating BaO-plane to the outer carbonate overlayer, was found to result in a significant stabilization of the system (within 5 meV) which indicates that the BaO-terminated surface with the full carbonate overlayer may be a metastable state. Nevertheless, further Ba-diffusion is required for the formation of $BaCO_3$ particles on the surface. Barium diffusion in $BaZrO_3$ is associated with an activation energy of about 4 eV as Ba^{2+} migrates through a square planar configuration of Zr^{4+} based on experimental and computational studies.[41] The extent of $BaCO_3$ formation on bulk $BaZrO_3$ material in CO_2-contining atmospheres is therefore limited by slow diffusion and not expected to be significant at lower temperatures.

DOI: 10.1021/acs.jpcc.7b08223
J. Phys. Chem. C 2018, 122, 307−314

5. CONCLUSION

BaO-terminated $BaZrO_3$ (0 0 1) exhibits strong affinity for CO_2 by chemisorption of carbonate species. The obtained thermodynamics of carbonate adsorption implies that the surface will be fully covered by a carbonate overlayer under ambient conditions containing 400 ppm of CO_2 and that significant coverage may be retained up to 2000 K under 1 bar CO_2. Migration of barium from the $BaZrO_3$ surface to the carbonate overlayer at the onset of $BaCO_3$ formation was found to be energetically favorable and feasible at ambient temperature with a low activation barrier. However, the formation of $BaCO_3$ precipitates at the surface would be limited by comparatively slow bulk diffusion of barium in $BaZrO_3$. The potential for bulk solubility of interstitial carbon in the form of carbonate species was considered and found to be negligible in acceptor-doped $BaZrO_3$.

AUTHOR INFORMATION

Corresponding Author

*Email: jonathan.polfus@sintef.no.

ORCID

Jonathan M. Polfus: 0000-0002-8975-185X

Notes

The authors declare no competing financial interest.

ACKNOWLEDGMENTS

We acknowledge financial support from the Research Council of Norway through the FOXCET project (Nano2021, 228355) and the Norwegian CCS research center for environmentally friendly energy (FME NCCS, 257579). Computational resources were provided through the Norwegian Metacenter for Computational Science (NOTUR) under Project No. nn9259k. B.Y. and H.L.T. acknowledge support from the Department of Energy, Basic Energy Science (Award No. DESC0002633).

REFERENCES

(1) Yan, N.; Zeng, Y.; Shalchi, B.; Wang, W.; Gao, T.; Rothenberg, G.; Luo, J. Discovery and Understanding of the Ambient-Condition Degradation of Doped Barium Cerate Proton-Conducting Perovskite Oxide in Solid Oxide Fuel Cells. *J. Electrochem. Soc.* **2015**, *162* (14), F1408−F1414.

(2) Kogler, M.; Köck, E. M.; Klötzer, B.; Perfler, L.; Penner, S. Surface Reactivity of YSZ, Y_2O_3, and ZrO_2 toward CO, CO_2, and CH_4: A Comparative Discussion. *J. Phys. Chem. C* **2016**, *120* (7), 3882−3898.

(3) Yu, Y.; Mao, B.; Geller, A.; Chang, R.; Gaskell, K.; Liu, Z.; Eichhorn, B. W. CO_2 Activation and Carbonate Intermediates: An Operando AP-XPS Study of CO_2 Electrolysis Reactions on Solid Oxide Electrochemical Cells. *Phys. Chem. Chem. Phys.* **2014**, *16*, 11633−11639.

(4) Wu, Z.; Li, M.; Overbury, S. H. On the Structure Dependence of CO Oxidation over CeO_2 Nanocrystals with Well-Defined Surface Planes. *J. Catal.* **2012**, *285* (1), 61−73.

(5) Feng, Z. a.; Machala, M. L.; Chueh, W. C. Surface Electrochemistry of CO_2 Reduction and CO Oxidation on Sm-Doped CeO_{2-x}: Coupling between Ce^{3+} and Carbonate Adsorbates. *Phys. Chem. Chem. Phys.* **2015**, *17* (18), 12273−12281.

(6) Feng, Z. A.; Balaji Gopal, C.; Ye, X.; Guan, Z.; Jeong, B.; Crumlin, E.; Chueh, W. C. Origin of Overpotential-Dependent Surface Dipole at CeO_{2-x}/Gas Interface during Electrochemical Oxygen Insertion Reactions. *Chem. Mater.* **2016**, *28* (17), 6233−6242.

(7) Kreuer, K. D. Proton Conducting Oxides. *Annu. Rev. Mater. Res.* **2003**, *33* (1), 333−359.

(8) Norby, T.; Widerøe, M.; Glöckner, R.; Larring, Y. Hydrogen in Oxides. *Dalt. Trans.* **2004**, *349*, 3012−3018.

(9) Duan, C.; Tong, J.; Shang, M.; Nikodemski, S.; Sanders, M.; Ricote, S.; Almansoori, A.; O'Hayre, R. Readily Processed Protonic Ceramic Fuel Cells with High Performance at Low Temperatures. *Science* **2015**, *349* (6254), 1321−1326.

(10) Malerød-Fjeld, H.; Clark, D.; Yuste-Tirados, I.; Zanón, R.; Catalán-Martinez, D.; Beeaff, D.; Morejudo, S. H.; Vestre, P. K.; Norby, T.; Haugsrud, R.; et al. Thermo-Electrochemical Production of Compressed Hydrogen from Methane with near-Zero Energy Loss. *Nat. Energy* **2017**, *2*, 1−9.

(11) Fabbri, E.; D'Epifanio, A.; Di Bartolomeo, E.; Licoccia, S.; Traversa, E. Tailoring the Chemical Stability of $Ba(Ce_{0.8-x}Zr_x)Y_{0.2}O_{3-\delta}$ Protonic Conductors for Intermediate Temperature Solid Oxide Fuel Cells (IT-SOFCs). *Solid State Ionics* **2008**, *179* (15−16), 558−564.

(12) Ryu, K. H.; Haile, S. M. Chemical Stability and Proton Conductivity of Doped $BaCeO_3$-$BaZrO_3$ Solid Solutions. *Solid State Ionics* **1999**, *125* (1), 355−367.

(13) Sažinas, R.; Bernuy-López, C.; Einarsrud, M.-A.; Grande, T. Effect of CO_2 Exposure on the Chemical Stability and Mechanical Properties of $BaZrO_3$-Ceramics. *J. Am. Ceram. Soc.* **2016**, *99* (11), 3685−3695.

(14) Mei, D. Density Functional Theory Study of Surface Carbonate Formation on BaO (0 0 1). *J. Phys. Chem. C* **2010**, *114* (1), 1867−1874.

(15) Jensen, M. B.; Pettersson, L. G. M.; Swang, O.; Olsbye, U. CO_2 Sorption on MgO and CaO Surfaces: A Comparative Quantum Chemical Cluster Study. *J. Phys. Chem. B* **2005**, *109* (35), 16774−16781.

(16) Shen, J.; Kobe, J. M.; Chen, Y.; Dumesic, J. A. Synthesis and Surface Acid/Base Properties of Magnesium-Aluminum Mixed Oxides Obtained from Hydrotalcites. *Langmuir* **1994**, *10* (10), 3902−3908.

(17) Solis, B. H.; Cui, Y.; Weng, X.; Seifert, J.; Schauermann, S.; Sauer, J.; Shaikhutdinov, S.; Freund, H.-J. Initial Stages of CO_2 Adsorption on CaO: A Combined Experimental and Computational Study. *Phys. Chem. Chem. Phys.* **2017**, *19* (6), 4231−4242.

(18) Baniecki, J. D.; Ishii, M.; Kurihara, K.; Yamanaka, K.; Yano, T.; Shinozaki, K.; Imada, T.; Nozaki, K.; Kin, N. Photoemission and Quantum Chemical Study of $SrTiO_3$(001) Surfaces and Their Interaction with CO_2. *Phys. Rev. B: Condens. Matter Mater. Phys.* **2008**, *78* (19), 1−12.

(19) Hammami, R.; Batis, H.; Minot, C. Combined Experimental and Theoretical Investigation of the CO_2 Adsorption on $LaMnO_{3+y}$ Perovskite Oxide. *Surf. Sci.* **2009**, *603* (20), 3057−3067.

(20) Shen, Y.; Wang, W.; Wang, X.; Zhou, Z.; Fei, W. First-Principles Study of CO_2 Adsorption on KNTN (0 0 1). *Appl. Surf. Sci.* **2014**, *308*, 269−274.

(21) Polo-Garzon, F.; Yang, S. Z.; Fung, V.; Foo, G. S.; Bickel, E. E.; Chisholm, M. F.; Jiang, D. E.; Wu, Z. Controlling Reaction Selectivity through the Surface Termination of Perovskite Catalysts. *Angew. Chem., Int. Ed.* **2017**, *56* (33), 9820−9824.

(22) Kröger, F. A.; Vink, H. J. Relations between the Concentrations of Imperfections in Crystalline Solids. *Solid State Phys.* **1956**, *3* (C), 307−435.

(23) Baniecki, J. D.; Ishii, M.; Kurihara, K.; Yamanaka, K.; Yano, T.; Shinozaki, K.; Imada, T.; Kobayashi, Y. Chemisorption of Water and Carbon Dioxide on Nanostructured $BaTiO_3$−$SrTiO_3$ (001). *J. Appl. Phys.* **2009**, *106* (5), 54109.

(24) Cheng, Z.; Sherman, B. J.; Lo, C. S. Carbon Dioxide Activation and Dissociation on Ceria (110): A Density Functional Theory Study. *J. Chem. Phys.* **2013**, *138* (1).01470210.1063/1.4773248

(25) Hahn, K. R.; Iannuzzi, M.; Seitsonen, A. P.; Hutter, J. Coverage Effect of the CO2 Adsorption Mechanisms on CeO_2 (111) by First Principles Analysis. *J. Phys. Chem. C* **2013**, *117* (4), 1701−1711.

(26) Albrecht, P. M.; Jiang, D. E.; Mullins, D. R. CO_2 Adsorption as a Flat-Lying, Tridentate Carbonate on CeO_2 (100). *J. Phys. Chem. C* **2014**, *118* (17), 9042−9050.

DOI: 10.1021/acs.jpcc.7b08223
J. Phys. Chem. C 2018, 122, 307−314

(27) Huang, M.; Fabris, S. CO Adsorption and Oxidation on Ceria Surfaces from DFT+U Calculations. *J. Phys. Chem. C* **2008**, *112* (23), 8643−8648.
(28) Ho, J.; Heifets, E.; Merinov, B. Ab Initio Simulation of the $BaZrO_3$ (001) Surface Structure. *Surf. Sci.* **2007**, *601* (2), 490−497.
(29) Kim, J.-S.; Kim, Y.-C. Equilibrium Crystal Shape of $BaZrO_3$ and Space Charge Formation in the (011) Surface by Using Ab-Initio Thermodynamics. *J. Korean Phys. Soc.* **2017**, *70* (1), 75−80.
(30) Blöchl, P. E. Projector Augmented-Wave Method. *Phys. Rev. B: Condens. Matter Mater. Phys.* **1994**, *50* (24), 17953−17979.
(31) Perdew, J.; Burke, K.; Ernzerhof, M. Generalized Gradient Approximation Made Simple. *Phys. Rev. Lett.* **1996**, *77* (18), 3865−3868.
(32) Kresse, G.; Joubert, D. From Ultrasoft Pseudopotentials to the Projector Augmented-Wave Method. *Phys. Rev. B: Condens. Matter Mater. Phys.* **1999**, *59* (3), 1758−1775.
(33) Grimme, S. Semiempirical GGA-Type Density Functional Constructed with a Long-Range Dispersion Correction. *J. Comput. Chem.* **2006**, *27* (15), 1787−1799.
(34) Atkins, P. W. *Physical Chemistry*, 6th ed.; Oxford University Press: Oxford, 1998.
(35) Chase, M. NIST-JANAF Thermochemical Tables. *J. Phys. Chem. Ref. Data*, 4th ed.; NIST, 1998; Monograph No. 9.
(36) Bale, C. W.; Chartrand, P.; Degterov, S. A.; Eriksson, G.; Hack, K.; Ben Mahfoud, R.; Melançon, J.; Pelton, A. D.; Petersen, S. FactSage Thermochemical Software and Databases. *CALPHAD: Comput. Coupling Phase Diagrams Thermochem.* **2002**, *26* (2), 189−228.
(37) Cornu, D.; Guesmi, H.; Krafft, J. M.; Lauron-Pernot, H. Lewis Acido-Basic Interactions between CO_2 and MgO Surface: DFT and DRIFT Approaches. *J. Phys. Chem. C* **2012**, *116* (11), 6645−6654.
(38) Chaney, J.; Santillán, J. D.; Knittle, E.; Williams, Q. A High-Pressure Infrared and Raman Spectroscopic Study of BaCO3: The Aragonite, Trigonal and Pmmn Structures. *Phys. Chem. Miner.* **2015**, *42*, 83−93.
(39) Polfus, J. M.; Bjørheim, T. S.; Norby, T.; Bredesen, R. Surface Defect Chemistry of Y-Substituted and Hydrated $BaZrO_3$ with Subsurface Space-Charge Regions. *J. Mater. Chem. A* **2016**, *4*, 7437−7444.
(40) Kim, J.-S.; Yang, J.-H.; Kim, B.-K.; Kim, Y.-C. Proton Conduction at BaO-Terminated (001) $BaZrO_3$ Surface Using Density Functional Theory. *Solid State Ionics* **2015**, *275*, 19−22.
(41) Sažinas, R.; Sakaguchi, I.; Hasle, I.; Polfus, J. M.; Haugsrud, R.; Einarsrud, M.-A.; Grande, T. Tracer Diffusion of ^{96}Zr and ^{134}Ba in Polycrystalline $BaZrO_3$. *Phys. Chem. Chem. Phys.* **2017**, *19*, 21878−21886.

DOI: 10.1021/acs.jpcc.7b08223
J. Phys. Chem. C 2018, 122, 307−314